Three-dimensional printing of highly conductive polymer nanocomposites for EMI shielding applications

Kambiz Chizari [a], Mohammad Arjmand [b], Zhe Liu [a], Uttandaraman Sundararaj [b,*], Daniel Therriault [a,*]

[a] Laboratory for Multiscale Mechanics (LM2), Center for Applied Research on Polymers (CREPEC), Department of Mechanical Engineering, Polytechnique Montréal, Montréal, Quebec, H3C 3A7, Canada

[b] Polymer Processing Group (PPG), Department of Chemical and Petroleum Engineering, University of Calgary, Calgary, Alberta, T2N1N4, Canada

* Corresponding authors

E-mail addresses: ut@ucalgary.ca, daniel.therriault@polymtl.ca (D. Therriault).

Abstract

Here we applied three-dimensional (3D) printing of conductive microstructures for the functional optimization of lightweight and semi-transparent electromagnetic interference (EMI) shields. Highly conductive 3D printable inks with electrical conductivities up to ~5000 S m^{-1} were fabricated from carbon nanotubes/polylactic acid (CNT/PLA) nanocomposites. Solvent-cast 3D printing enabled us to fabricate conductive scaffold microstructures and investigate the influence of various important structural parameters (i.e., inter-filament spacing, number of layers and printing patterns) on their transparency and EMI shielding effectiveness. The results revealed a significant improvement of the specific EMI shielding effectiveness of CNT/PLA nanocomposites printed as 3D scaffolds compared to CNT/PLA hot-pressed in solid forms (~70 vs ~37 dB g^{-1} cm^3). The transparency of the scaffolds could vary from ~0% to ~75% by modifying their printing patterns and inter-filament spacing. To the best of our knowledge the conductivity of the fabricated ink is the highest among the other reported 3D printable polymer composite inks and this is the first reported systematic study on EMI shielding using a 3D printing technique. These results are highly beneficial for the fabrication and structural optimization of EMI shields where light and/or transparent structures are advantageous, such as in aerospace systems, portable electronic devices or smart fabrics.

1. Introduction

Conductive polymer nanocomposites (CPNs) are composed of conductive nanofillers (e.g. carbon nanotubes, graphene and metal-lic nanowires) dispersed in a polymer matrix. The utilization of CPNs for electromagnetic interference (EMI) shielding [1–5], lightning strike protection in airplanes [6,7], sensors [8,9], and in the field of electronics [10–13] have been reported. Among diverse applications of CPNs, EMI shielding is especially demanding due to the industrial requirements of lightweight and highly conductive materials [3]. Emitted electromagnetic (EM) waves from electron-ics can potentially be hazardous to people's health and interfere with the operation of electronic devices [14]. In this regard, the proliferating market of electronics has heightened the necessity to resolve the growing EMI issues.

Metals are common materials employed as EMI shields [15]; however, metallic shields have drawbacks like corrosion, high cost, high weight, and expensive to process. Hence, during the last decade, technological breakthroughs and research focus in the field of EMI shielding materials have been intensely directed towards the development of CPNs [16–18]. CPNs benefit from the intrinsic properties of polymers (i.e., light weight, low cost, corrosion resistance, and easy processing) combined with tuneable electrical conductivity derived from the adjustable filler morphology (i.e. conductive network) within the polymer matrix [19]. Electrical conductivity is a key parameter for effective EMI shielding materials [4,20]. Most of common polymers are inherently insulative; however, embedding sufficient amount of conductive nanofiller into polymer matrices leads to the formation of conductive networks across the nanocomposite. This transforms the whole nanocomposite into a conductive material. Conduction via physical contacts between conductive nanofillers in combination with electron tunnelling and hopping between conductive nanofillers are the main mechanisms for the electron transference in CPNs [21,22].

Forming CPNs can be achieved by different common methods such as injection molding, compression molding or solvent casting [17,23]. Recently, three-dimensional (3D) printing method has also attracted the attention of researchers due to its capability for fabrication of complex shapes at relatively high speed since no mold fabrication is required [24,25]. As yet, different types of 3D printing (3DP) method, such as fused deposition modeling (FDM) [26–28], selective laser sintering (SLS) [29], stereolithography (SLA) [30,31], UV assisted 3DP (UV3DP) [32,33] and solvent cast 3DP (SC3DP) [34,35] have been developed. Among the different 3D printing technologies, FDM is the most frequently used 3D printing method [36]. In this method, the polymer melt extrudes out of a heated nozzle to form a 3D shape by layer-by-layer deposition on a platform. Fabrication of conductive structures is challenging using FDM method since metals have very high melting temperatures and CPNs with a high concentration of conductive fillers have high viscosity at their melting point, obstructing the printing nozzle and hampering the printing process.

In SLS method, the initial material is in a form of powder and the 3D shape forms when the powder particles attach to each other due to the sintering of the powder particles caused by the heat of a focalized laser. The printing powder can be metal or CPN particles. The main shortcoming of SLS to the other 3D printing methods is the complexity, the high price of the printing equipment, and the lack of control on the alignment of the nanofillers dispersed in the polymer matrix.

In UV3DP method, the UV light is focalized on the tip of the printing nozzle and cures the UV-curable polymer while the polymer extrudes out of the nozzle [37]. SLA is based on the local polymerization of a thermoset polymer by a laser beam. Printing conductive materials with these two methods are highly challenging since adding nanofillers inside a thermoset polymer can hinder the polymerization and cross-linking processes. SC3DP functions based on the solidification of the polymer-solvent mix due to the rapid evaporation of the solvent during the printing process [34,35]. The advantages of this method compared to the above-discussed 3D printing techniques are its simplicity, low price, and the possibility of adjusting the ink's viscosity by modifying its solvent concentration, enabling us to print various types of nanocomposites with high concentration of the nanofillers. The details related to SC3DP method are previously published [34,35].

In this paper, we report the fabrication of highly conductive CPNs used as the ink for SC3DP method. Employing the fabricated CPNs, we developed 3D printed conductive grid-like configurations and investigated the effect of their structural parameters (i.e., inter-filament spacing, number of printed layers and printing patterns) on their EMI shielding performance and transparency. The specific EMI shielding of the CPNs in different structures were also investigated to provide more insight about the structural effects on the EMI SE considering the mass of the EMI shield.

2. Experimental

2.1. Nanocomposite and ink preparation

Multi-walled carbon nanotube/polylactic acid (CNT/PLA) nanocomposites were prepared by mixing a solution of PLA (PLA 4032D, Natureworks LLC) dissolved in dichloromethane (DCM) with carbon nanotubes (Nanocyl^{TM} NC7000, Sambreville, Belgium) using ball mill mixing method (SPEX SamplePrep 8000 M Mixer/Mill) [38]. DCM dissolves well the PLA matrix and the high volatility of DCM makes it a suitable solvent for the SC3DP ink [34,35]. First, PLA was dissolved in DCM at a concentration of 10 wt.% by placing PLA pellets in DCM solvent for about 24 h in a well-sealed glass vial. The PLA-DCM solution was poured inside a ball mill vial together with the required amount of CNTs (depending on the desired wt.% of CNT/PLA) and ball milled for 30 min. After the mixing, CNT/PLA-DCM suspensions with CNT contents of <20 wt.% were dried at room temperature for 24 h. The dried CNT/PLA nanocomposites were dissolved in DCM to make a CNT/PLA-DCM suspension with CNT/PLA to DCM concentration of 30 wt.% as an ink compatible for SC3DP method. In the case of CNT/PLA nanocomposites with CNT content of ≥20 wt.%, the CNT/PLA-DCM suspension was used as the printing ink directly after mixing due to the difficulties of dissolving dried CNT/PLA with high CNT concentration in DCM solvent [25]. The maximum CNT/PLA concentration used for fabrication of nanocomposites was 40 wt.%, in which the texture of the ink becomes like a wet powder rather than a viscous liquid suitable for 3D printing ink.

2.2. 3D printing of scaffolds structures

The CNT/PLA-DCM ink was poured into a syringe, which was then mounted on the head of a dispensing robot (Fisnar I&J2200-4). The printing patterns were designed and transferred to the printing robot using JR Points software made by Janome Industrial Equipment. The syringes and micronozzles (inner diameter of 200 μm) were supplied by Nordson EFD Co. The displacement rate of the robot was in the range of 0.3–1.0 mm s^{-1} depending on the CNT concentration in the ink. The extrusion pressure was controlled using a pressure regulator (HP-7X, EFD), and was set in the range of 2.1–4.2 MPa.

2.3. Fabrication of solid samples

The CNT/PLA nanocomposites with different CNT concentrations fabricated by ball mill mixing method were compression molded under the pressure of 38 MPa for 5 min using a Carver compression molder (Carver Inc., Wabash, IN). A metallic mold with dimensions of $22.9 \times 10.2 \times 0.4\,mm^3$ was used to form rectangular shaped solid samples in order to cover the X-band waveguide window of the EMI network analyzer.

2.4. Electrical conductivity measurements

The electrical conductivity tests were performed on the solid samples. The surface of the samples was wiped with ethanol to remove impurities prior to the conductivity measurements. For nanocomposites with electrical conductivities more than 10^{-2} S m^{-1}, the conductivity measurements were carried out according to ASTM 257-75 using a Loresta GP resistivity meter (MCPT610 model, Mitsubishi Chemical Co., Japan) connected with a four-point probe. A Keithley 6517A electrometer connected to a Keithley 8009 test fixture (Keithley Instruments, USA) was used for the measurements of the nanocomposites with conductivities less than 10^{-2} S m^{-1}. The reported conductivities and the error bars are the average and the standard deviation of six conductivity measurements for each concentration.

2.5. EMI shielding testing

EMI shielding measurements were performed over the X-band (8.2–12.4 GHz) frequency range using an E5071C network analyzer (ENA series 300 KHz–20 GHz). EMI shielding effectiveness (EMI SE) is defined as the logarithm of the ratio of the incident power to the transmitted power and is expressed in dB:

$$\text{EMI SE} = 10 \log \left(\frac{P_i}{P_o} \right) \quad (1)$$

where P_i is the incident power and P_o is the transmitted power.

The EMI SE and error bar values are the average and standard deviation values of the overall EMI SE data over the X-band frequency range, respectively. The rectangular scaffolds and solid samples were placed between two X-band flanges, connected to the separate waveguide ports of the network analyzer. The network analyzer sent an electromagnetic wave onto the sandwiched sample and the powers of the incident, reflected and transmitted waves were measured by three wave detectors to calculate EMI SE. EMI SE is calculated as the following:

$$SE_R = 10 \times \log\left(\frac{1}{1-R}\right) \quad (2)$$

$$SE_A = 10 \times \log\left(\frac{1-R}{T}\right) \quad (3)$$

$$EMISE = SE_R + SE_A \quad (4)$$

where SE_R, SE_A and EMI SE are the shielding by reflection, shielding by absorption and overall shielding, respectively. R and T are reflectance and transmittance, respectively. Further information regarding the EMI shielding measurement can be found elsewhere [39].

2.6. Transparency tests

A Lambda1050 (Perkin Elmer) double-beam spectrophotometer equipped with a 150 mm diameter, integrating sphere was used to obtain the transparency of the scaffold structures. The transmittance of the light with a wavelength ranging from 300 to 850 nm was tested with a 5 nm step increment. The reported transmittance values and the error bars are resulted from the average and standard deviation of the transmittance over the tested wavelength range, respectively.

3. Results and discussion

Mixing CNT with a solution of PLA-DCM via ball mill mixing method enabled us to fabricate CNT/PLA nanocomposites with CNT concentrations up to 40 wt.%. Based on our experience of CNT/PLA fabrication using various mixing methods such as solution mixing or melt extrusion [40], the ball mill mixing method was more suitable for the synthesis of CNT/PLA nanocomposites with high CNT concentrations (>10 wt.%). This is mainly due to the fact that the problems associated with the high viscosity of the mixing materials and poor dispersion of CNTs in DCM at high CNTs concentrations, hinder the extrusion and solution mixing processes, respectively.

Fig. 1a shows the electrical conductivity (σ) of the solid CNT/PLA nanocomposites as a function of CNT concentration. It was observed that by increasing the CNT concentration from 0 to 40 wt.%, the electrical conductivity of the nanocomposites increased from ~1.4E − 14 to ~1.7E + 4 S m^{-1}. The electrical conductivity of the CNT/PLA nanocomposites obtained by ball mill mixing method using 5 wt.% CNT, i.e. 340 S m^{-1}, was significantly more than the ones obtained via solution mixing (~4 S m^{-1}) or extrusion (~25 S m^{-1}) using the same materials [40], endorsing the superiority of ball mill compared to the other composite mixing techniques. A comparison of the electrical conductivities obtained for the CNT/PLA nanocomposites to the other values reported for conductive CNT/polymer nanocomposites with high CNT loadings (≥10 wt.%) (Table S1 and Fig. 1b) shows the high performance of the nanocomposite fabrication process used in this work. Further information related to the reported electrical conductivity of CNT/polymer nanocomposites can be found elsewhere [41,42].

In order to estimate the electrical percolation threshold for CNT/PLA nanocomposites, we employed the percolation theory [43], wherein the power law (Eq. (5)) was used to fit the electrical conductivity data.

$$\sigma = \sigma_0(\nu - \nu_c)^t \quad (5)$$

In the above equation, σ_0 is a scaling factor, ν is the nanofiller volume fraction, ν_c is the electrical percolation threshold volume fraction and t is a critical exponent. Given the density of CNT (1.75 g cm^{-3}) and PLA (1.25 g cm^{-3}), the linear regression data fitting (Fig. 1c) gives percolation threshold, ν_c, to be 0.03 vol% (0.04 wt.%). Although lower percolation thresholds have been reported [42,44], 0.04 wt.% is significantly lower than the typical value of ~0.1 wt.% calculated for the percolation threshold of CNT/polymer systems with an optimized CNT dispersion [42,45].

Fig. 1d shows the SC3DP method enabled us to print scaffold structures with various structural parameters, i.e. inter-filament spacing (IFS), the number of layers and printing patterns. Printing of the conductive ink with CNT concentration up to 30 wt.% was possible by this method, as it does not deal with the problems related to melting of highly concentrated nanocomposites. The scaffolds printed with 40 wt.% CNT were too fragile resulting in partial rupturing of scaffolds during the EMI shielding tests. Hence, they can hardly be used for EMI shielding applications due to their low mechanical strength originating from high filler concentration. The electrical conductivity of the nanocomposite used as 3D printing ink was as high as ~5000 S m^{-1} (CNT: 30 wt.%), which is notably high compared to other reported electrical conductivities related to CPNs useful for 3D printing (e.g. <100 S m^{-1} [46], <1 S m^{-1} [47], and ~10 S m^{-1} [48]).

SEM images of the fabricated scaffolds are shown in Fig. 1e. Three different configurations were printed and named open window, closed window, and zigzag structures. The printed filaments in the third and fourth layers of the closed window pattern are located in between the first and second layers, closing the windows formed from the first and second layers. The printing trajectories of these patterns are shown in Fig. S1. Depending on the structural pattern, the transparency of the samples can vary. Fig. 1f shows an image covered by 3 different printed scaffolds. The visibility through scaffold with open window structure is much more compared to the closed window structure, while they have similar mass. Therefore, simply by modifying the 3D printing pattern, the transparency of the structure can be changed using similar amount of material.

Fig. 2a shows the variation of EMI SE as a function of CNT concentration for the scaffolds (printed in four layers, open window pattern and IFS of 0.7 mm) and solid structures. The EMI SE of the CNT/PLA with CNT concentrations up to 5 wt.% is shown in Fig. S2 to better see nanocomposites' EMI SE at low CNT concentrations. The EMI SE of the CNT/PLA shields in both types of structures, scaffold and solid forms, increased by increasing the CNT concentration. For the solid samples, EMI SE increased to about 47 and 55 dB for CNT concentrations of 20 and 30 wt.%, respectively. In order to test the reproducibility of the results, three identical scaffolds with the CNT percentage of 20 wt.% were fabricated and their EMI SE was measured. The results showed about 14% variation between the EMI SE of the scaffolds made with similar configurations. A comparison between the EMI SE of the fabricated CNT/PLA in solid form to the values reported in the literature for CNT/polymer with high CNT loading (≥10 wt.%), demonstrates the significance of the present work considering the thickness of the characterized nanocomposite films (Table S2).

The increase in EMI shielding with CNT content can be attributed to the increase in shielding by both EM reflection and absorption [16]. When an EM wave hits a conductive shield, a fraction of the EM wave is reflected off the shield due to interaction with the surface free charge carriers (impedance mismatch between two media) and a fraction infiltrates through the shield with its energy dissipated via absorption. Shielding by reflection for mate-

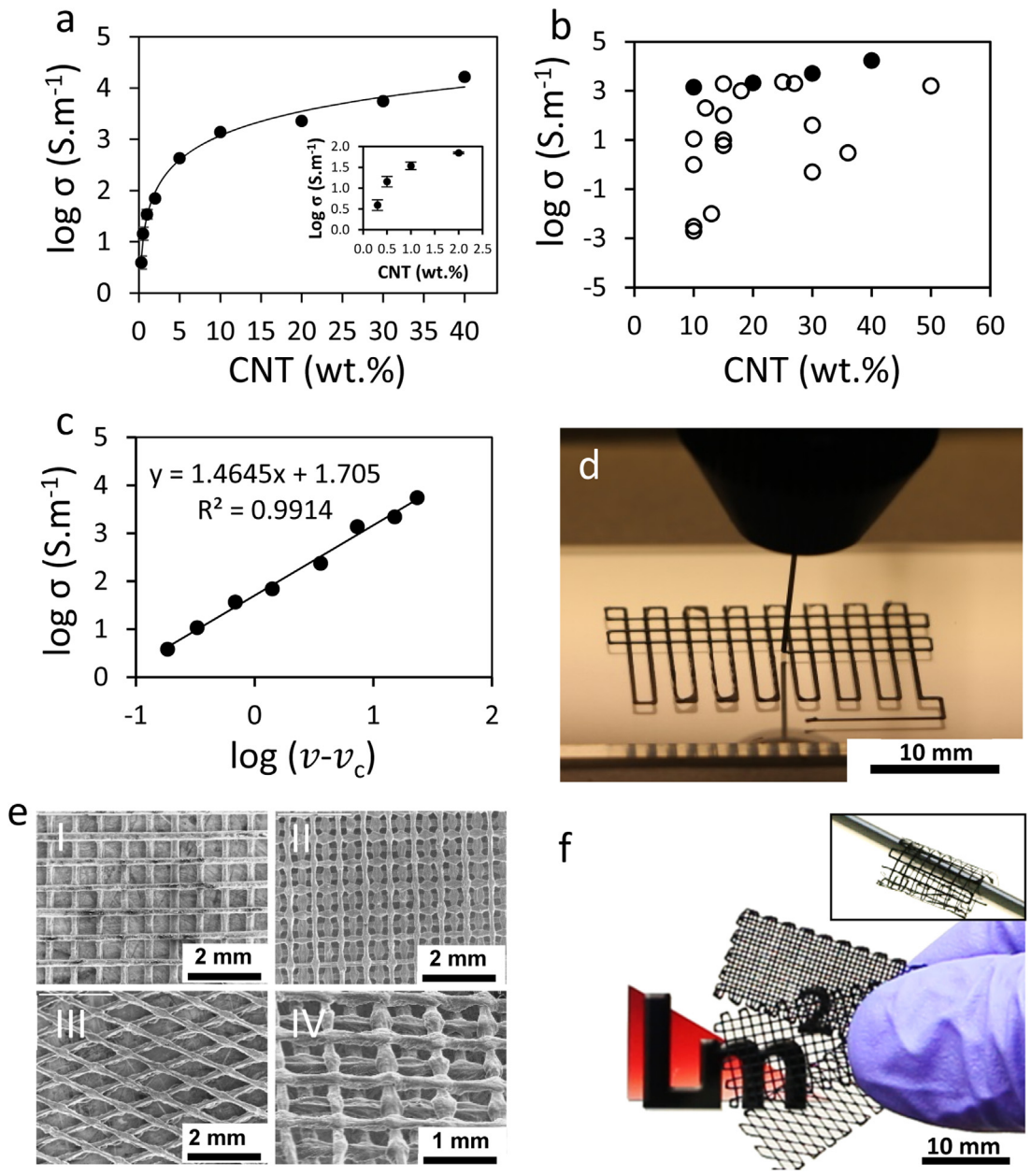

Fig. 1. (a) Electrical conductivity of the CNT/PLA nanocomposites with respect to CNT concentration. The conductivity of CNT/PLA can reach to ~10^4 S m^{-1} by increasing the CNT concentration to 40 wt.%. Inset shows the conductivity of CNT/PLA with CNT concentration up to 2 wt.%. (b) Electrical conductivity of the CNT/polymer nanocomposites with high CNT loadings (≥10 wt.%) based on the literature cited in Table S1. The filled circles (●) show the conductivity of CNT/PLA obtained in the present work and the empty circles (○) are the ones reported in the literature. (c) Plot of log σ against log (v–v_c) according to the power law equation with linear regression data fitting. To obtain the best linear fit for log σ against log (v–v_c), the value of v_c was incrementally decreased below the lowest volume fraction in the conductive region until the highest correlation factor R^2 was obtained. The data fitting suggests that the system electrical percolation threshold is 0.03 vol.%. (d) 3D printing of scaffolds by SC3DP method using a nozzle with 200 μm inner diameter. (e) Top view SEM images of scaffolds fabricated in different patterns; I: Open window, II: Closed window, III: Zigzag and IV: 45° angle view of closed window pattern. (d) Three 4-layered printed scaffolds with different printed patterns but similar IFS, showing the transparency of the scaffolds. The Zigzag and open window patterns showed much better transparency compared to the closed window pattern. The inset photo is a scaffold printed in 2 layers wrapped around a metal bar with a diameter of 2.5 mm showing its flexibility.

rials is proportional to $\frac{\sigma}{\mu}$, where μ is the magnetic permeability. This proportionality implies that materials with higher conductivity present higher reflection, while the magnetic materials reduce shielding by reflection. Shielding by absorption for a conductive material is proportional to $\sigma \cdot \mu$, i.e., materials with high conductivity and high magnetic permeability attenuate EM wave efficiently [49,50]. In fact, absorption attenuates EM wave through interaction with free charge carriers and/or electric/magnetic dipoles. It is worth noting that the employed CNTs are non-magnetic; therefore, they mainly attenuate EM wave by their free charge carriers.

For the scaffold samples, the EMI SE increased to ~30 dB by increasing the percentage of CNTs to 20 wt.%. Adding more amounts of CNTs to the nanocomposite formula did not improve the EMI SE, showing that it reaches a plateau in the range of CNT concentration between 20 and 30 wt.%. This can be attributed to the presence of spacing in the 3D printed CPNs scaffolds, allowing a small portion

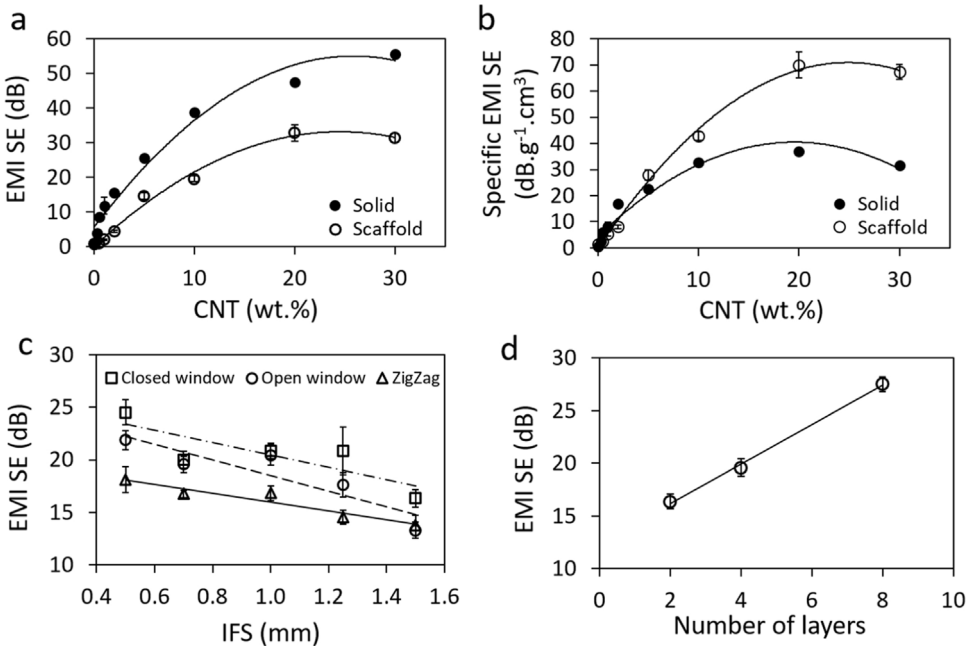

Fig. 2. (a) Average EMI SE and (b) specific EMI SE of the solid and scaffold structures over the X-band frequency range as a function of CNT loading. The solid samples had 0.4 mm thickness, and the scaffold samples were printed with an IFS of 0.7 mm in four layers with open window pattern. (c) The graph of EMI SE as a function of IFS of the scaffolds with different printing patterns (CNT/PLA concentration: 10 wt.%) showing a slight decrease in EMI SE by increasing the IFS. (d) EMI SE of scaffolds with IFS of 0.7 mm and CNT concentration of 10 wt.% as a function of the number of printing layers in open window pattern. The EMI SE could be modified by changing the number of printed layers.

of electromagnetic wave (0.1% for EMI SE of 30 dB) passes through the sample.

Since the mass of the materials used as EMI shields is a crucial factor for various applications, such as in portable electronic devices and aircrafts, the EMI SE values of the solid and scaffold structures were normalized with respect to their density and referred to specific EMI SE (Fig. 2b). The density is calculated based on the total volume of the structures including the empty space [51–53]. Comparing Fig. 2a and b shows that increasing the CNT concentration in solid samples from 10% to 40% had positive effect on the EMI SE but not the specific EMI SE. It shows that the increase in density while increasing the CNT wt.%, due to the higher density of CNTs compared to PLA, could compensate the increase in EMI SE. Based on these results, increasing the CNT concentration for more than 10% might not have positive effect for the EMI shields where the solid form is required and the mass is an important factor for their application. The specific EMI SE of the scaffolds increased with a higher rate compared to the solid samples with the maximum of ~70 dB g^{-1} cm^3 and ~37 dB g^{-1} cm^3, respectively. At low CNT concentrations (<5 wt.%), the specific EMI SE of the scaffolds is slightly lower than the solid samples. The scaffolds with CNT concentration equal to or more than 5 wt.% show higher specific EMI SE values compared to the solid structures. The difference in the specific EMI SE of the solid and scaffold structures rose up with CNT content and increased to about 33 dB g^{-1} cm^3. Since the EMI SE of the scaffolds with CNT concentration of 20 wt.% is more than 30 dB and their specific EMI SE is about two times higher than the solid structures, they have a promising future as lightweight EMI shielding structures.

Fig. 2c demonstrates the influence of the scaffolds' IFS on their EMI SE characteristics. The EMI SE decreased slightly by increasing the IFS for all three types of the structural patterns. Normalizing the EMI SE of the scaffolds by their mass revealed no significant variation of the EMI SE/mass values by changing the IFS (Fig. S3). This shows that the decrease in EMI SE by increasing the IFS can be related to the reduced amount of conductive material for larger IFS, leading to less number of interacting free charge carriers.

Fig. 2d shows the influence of the variation in the number of layers in the scaffold structure on the EMI SE for the scaffold structures printed in an open window pattern with IFS of 0.7 mm and CNT concentration of 10 wt.%. EMI SE increased from 16 to about 28 dB by increasing the number of layers in scaffolds from 2 to 8. Based on these results, 3D printing of conductive materials enables us to adjust the EMI SE of the scaffold structures simply by manipulating the configuration, IFS, number of printed layers, etc. Depending on the desired application of the EMI shielding material, the most suitable configuration with the IFS and number of layers can be fabricated.

One of the main advantages of the scaffold structures over the solid EMI shielding structures is the semi-transparency of these grid-like structures, which can be useful for the applications where the transparency is an important key. The visible light transmittance of the scaffolds printed in four layers with IFS of 0.7 mm and CNT concentration of 10 wt.% as a function of their IFS is shown in Fig. 3a. Increasing the IFS increased the transparency of the scaffold structures to as high as ~75%. Since the CPN used for the EMI shielding is not transparent and the transparency originates from the grid-like structure, varying the structure changed the transparency and also the EMI SE. The open window and zigzag patterns had higher light transmittance compared to the closed window pattern. This can be due to the arrangement of the printed filaments in closed window pattern, blocking the passing light more than the other printed patterns (Fig. S1). Fig. 3b shows the EMI SE and transparency as a function of the IFS of the scaffolds. Lower IFS led to higher EMI SE but decreased transparency. In fact, by decreasing the IFS the filaments are closer to each other and more CNT/PLA filaments block the transmittance of the light. Comparing the EMI SE (Fig. 2c) and transmittance (Fig. 3a) of the scaffolds with different IFS revealed the possibility of increasing the transparency of these structures while maintaining their EMI SE constant by chang-

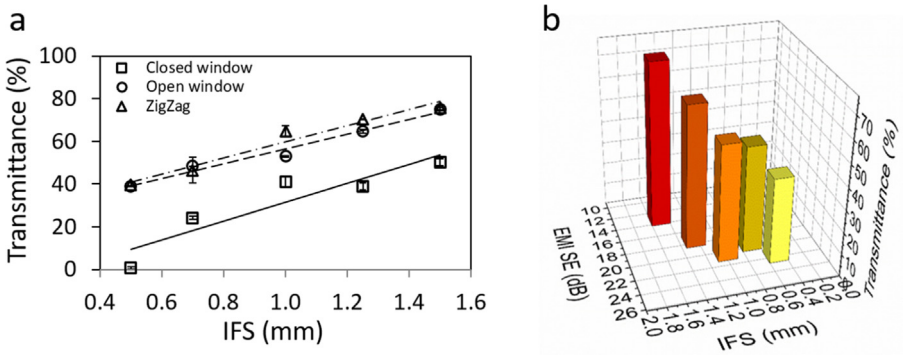

Fig. 3. (a) The transmittance of the scaffolds increased by increasing the IFS, since the distance between the filaments increased and lower total mass of CPNs was used for the equal surface exposed to light. Changing pattern from closed window to open window or zigzag, increased the light transmittance. (b) 3D graph showing EMI SE and transparency of the scaffolds, printed in open window pattern using the conductive ink with CNT concentration of 10%, as a function of their IFS. Depending on the desired transparency and EMI SE, the IFS and the printed pattern of the scaffold can be adjusted.

ing the printing patterns from closed window to open window. The difference in EMI SE of scaffolds printed in different patterns was relatively low, while their transmittance could rise from ~0 to ~40% (IFS: 0.5 mm). The transmittance of the scaffold with IFS of 0.7 mm could be doubled while maintaining the EMI SE value by changing the structural patterns from closed window to open window. Other interesting aspect of this study is the fact that by increasing the number of printed layers the EMI SE could be increased while maintaining the transparency of the scaffold (<5% reduction per layer). This is due to the fact that the transparency originates from the holes in grid-like configurations and not the nature of the material. In the case of solid structures, the transparency is highly dependent on the thickness of transparent films [37], so increasing the EMI SE by thickening the EMI shielding film decreases its transparency. Thus, this problem can be solved by altering the EMI shielding structures from solid to grid-like structures.

4. Conclusions

Highly conductive 3D printable ink with an electrical conductivity up to ~5000 S m^{-1} was obtained from CNT/PLA conductive nanocomposite. 3D printing was used to build conductive, light, and semi-transparent scaffold structures tested for EMI shielding application. The specific EMI SE of the printed scaffolds could reach to about two times more than the one for the solid form of the conductive CNT/PLA nanocomposite (~70 dB g^{-1} cm^3 vs ~37 dB g^{-1} cm^3). This is highly useful for EMI shields where lightweight material is beneficial such as in airplanes and portable electronic devices (e.g., laptops, cell phones and wearable electronics). 3D printing enabled us to demonstrate the influence of certain structural parameters such as IFS and number of printed layers on the EMI SE of the designed configurations. Decreasing IFS or increasing the number of scaffold layers increased the EMI SE. The results showed that the modification in the number of printed layers had a higher impact on the EMI SE compared to the IFS. Due to the semi-transparency of the scaffolds, originated from their grid-like structure, they are promising for EMI shielding applications where transparency is beneficial. The light transmittance of the scaffolds increased from ~0 to ~75% by changing the printing pattern from closed window to open window and increasing the IFS from 0.5 to 1.5 mm. For improving the 3D printing speed, reproducibility and practicality of the fabricated structures, the inks' rheological properties and the influence of printing parameters on the mechanical properties of the printed configurations will be investigated. It will be also useful to study and compare the specific EMI SE of the grid-like CPNs to the metallic mesh for their practical application as EMI shields. This study will be expanded to the structural optimization of more complex 3D printed structures, with different patterns along their thickness direction, for higher EMI SE and/or transparency. Combining the 3D printing technique with the numerical simulation tools can be one of the fastest way to validate the practicality of the data obtained in theory.

Acknowledgements

The authors acknowledge the financial support from Natural Sciences and Engineering Research Council of Canada (NSERC – grant number: RGPAS-446198-2013 and RGPIN/05503-2015). We would like to thank Dr. Richard Vernhes from École Polytechnique de Montréal for providing us technical assistance with the optical characterization. We also thank Dr. Shuang-Zhuang Guo for his technical assistance with the solvent-cast 3D printing method.

Appendix A. Supplementary data

Supplementary data associated with this article can be found, in the online version, at http://dx.doi.org/10.1016/j.mtcomm.2017.02.006.

References

[1] N. Li, Y. Huang, F. Du, X. He, X. Lin, H. Gao, Y. Ma, F. Li, Y. Chen, P.C. Eklund, Nano Lett. 6 (2006) 1141–1145.
[2] M. Arjmand, M. Mahmoodi, G.A. Gelves, S. Park, U. Sundararaj, Carbon 49 (2011) 3430–3440.
[3] F. Qin, C. Brosseau, J. Appl. Phys. 111 (2012) 061301.
[4] D. Chung, Carbon 39 (2001) 279–285.
[5] S. Celozzi, G. Lovat, R. Araneo, Electromagnetic Shielding, Wiley Online Library, 2008.
[6] M. Gagné, D. Therriault, Prog. Aerosp. Sci. 64 (2014) 1–16.
[7] P.J. Glatkowski, D.H. Landis, J.W. Piche, J.L. Conroy, Patent Number: US6986853 B2, (2006).
[8] X. Kang, Z. Mai, X. Zou, P. Cai, J. Mo, Anal. Biochem. 363 (2007) 143–150.
[9] K. Inpil, J.S. Mark, H.K. Jay, S. Vesselin, S. Donglu, Smart Mater. Struct. 15 (2006) 737.
[10] S. Bae, H. Kim, Y. Lee, X. Xu, J.-S. Park, Y. Zheng, J. Balakrishnan, T. Lei, H. Ri Kim, Y.I. Song, Y.-J. Kim, K.S. Kim, B. Ozyilmaz, J.-H. Ahn, B.H. Hong, S. Iijima, Nat. Nano 5 (2010) 574–578.
[11] G. Eda, M. Chhowalla, Nano Lett. 9 (2009) 814–818.
[12] S. Stankovich, D.A. Dikin, G.H.B. Dommett, K.M. Kohlhaas, E.J. Zimney, E.A. Stach, R.D. Piner, S.T. Nguyen, R.S. Ruoff, Nature 442 (2006) 282–286.
[13] J.A. Rogers, T. Someya, Y. Huang, Science 327 (2010) 1603–1607.
[14] N. Lawrentschuk, D.M. Bolton, Med. J. Aust. 181 (2004) 145–149.
[15] R. Salgarkar, Electromagnetic Compatibility (EMC) Shielding and Test Equipment Market by Type, MarketsandMarkets, 2015 www.marketsandmarkets.com.
[16] J.-M. Thomassin, C. Jérôme, T. Pardoen, C. Bailly, I. Huynen, C. Detrembleur, Mater. Sci. Eng. R-Rep. 74 (2013) 211–232.

[17] M. Arjmand, T. Apperley, M. Okoniewski, U. Sundararaj, Carbon 50 (2012) 5126–5134.
[18] A. Ameli, P. Jung, C. Park, Carbon 60 (2013) 379–391.
[19] M. Arjmand, M. Mahmoodi, S. Park, U. Sundararaj, J. Cell. Plast. 50 (2014) 551–562.
[20] S. Geetha, K. Satheesh Kumar, C.R. Rao, M. Vijayan, D. Trivedi, J. Appl. Polym. Sci. 112 (2009) 2073–2086.
[21] M. Trojanowicz, TrAC Trends Anal. Chem. 25 (2006) 480–489.
[22] M. Arjmand, K. Chizari, B. Krause, P. Pötschke, U. Sundararaj, Carbon 98 (2016) 358–372.
[23] M. Arjmand, U. Sundararaj, Compos. Sci. Technol. 118 (2015) 257–263.
[24] R.D. Farahani, M. Dubé, D. Therriault, Adv. Mater. 28 (2016) 5794–5821.
[25] K. Chizari, M.A. Daoud, A.R. Ravindran, D. Therriault, Small 12 (2016) 6076–6082.
[26] S. Scott Crump, Patent Number: US5121329, (1992).
[27] D.W. Hutmacher, Biomaterials 21 (2000) 2529–2543.
[28] D.T. Pham, R.S. Gault, Int. J. Mach. Tools Manuf. 38 (1998) 1257–1287.
[29] J.J. Beaman, C.R. Deckard, Patent Number: US4938816A, (1990).
[30] P.F. Jacobs, Stereolithography and Other RP&M Technologies: From Rapid Prototyping to Rapid Tooling, ASME Press, New York, 1996.
[31] X. Zhang, X.N. Jiang, C. Sun, Sens. Actuators A Phys. 77 (1999) 149–156.
[32] R. Farahani, L. Lebel, D. Therriault, J. Micromech. Microeng. 24 (2014) 055020.
[33] L.L. Lebel, B. Aissa, M.A.E. Khakani, D. Therriault, Adv. Mater. 22 (2010) 592–596.
[34] S.Z. Guo, F. Gosselin, N. Guerin, A.M. Lanouette, M.C. Heuzey, D. Therriault, Small 9 (2013) 4118–4122.
[35] S.-Z. Guo, M.-C. Heuzey, D. Therriault, Langmuir 30 (2014) 1142–1150.
[36] S.S. Crump, Patent Number: US5121329, (1992).
[37] M. Arjmand, A.A. Moud, Y. Li, U. Sundararaj, RSC Adv. 5 (2015) 56590–56598.
[38] K. Chizari, D. Therriault, Proceedings of the Tenth Joint Canada-Japan Workshop on Composites 2014, Vancouver, Canada, DES tech Publications, Inc., 2015, p. 214.
[39] M. Arjmand, Electrical Conductivity, Electromagnetic Interference Shielding and Dielectric Properties of Multi-walled Carbon Nanotube/Polymer Composites, University of Calgary, 2014, PhD Thesis.
[40] B.S. Talwar, K. Chizari, S. Guo, D. Therriault, ASME 2014 International Mechanical Engineering Congress and Exposition, American Society of Mechanical Engineers, 2014, V02BT02A046-V002BT002A046.
[41] M. González Sánchez, G. Mokry López, N. Morillas, J. Baselga Llidó, J. Pozuelo de Diego, Intech, 2016, pp. 297–321.
[42] Z. Spitalsky, D. Tasis, K. Papagelis, C. Galiotis, Prog. Polym. Sci. 35 (2010) 357–401.
[43] M. Weber, M.R. Kamal, Polym. Compos. 18 (1997) 711–725.
[44] C. Martin, J. Sandler, M. Shaffer, M.-K. Schwarz, W. Bauhofer, K. Schulte, A. Windle, Compos. Sci. Technol. 64 (2004) 2309–2316.
[45] W. Bauhofer, J.Z. Kovacs, Compos. Sci. Technol. 69 (2009) 1486–1498.
[46] G. Postiglione, G. Natale, G. Griffini, M. Levi, S. Turri, Compos. Part A Appl. Sci. Manuf. 76 (2015) 110–114.
[47] J. Czyżewski, P. Burzyński, K. Gaweł, J. Meisner, J. Mater. Process. Technol. 209 (2009) 5281–5285.
[48] S.J. Leigh, R.J. Bradley, C.P. Purssell, D.R. Billson, D.A. Hutchins, PLoS One 7 (2012) e49365.
[49] C.R. Paul, Introduction to e Lectromagnetic Compatibility, John Wiley & Sons Inc, New Jersey, 2006.
[50] K.L. Kaiser, Electromagnetic Shielding, CRC Press, Michigan, 2005.
[51] D.-X. Yan, P.-G. Ren, H. Pang, Q. Fu, M.-B. Yang, Z.-M. Li, J. Mater. Chem. 22 (2012) 18772–18774.
[52] A. Ameli, M. Nofar, S. Wang, C.B. Park, ACS Appl. Mater. Interfaces 6 (2014) 11091–11100.
[53] Z. Chen, C. Xu, C. Ma, W. Ren, H.M. Cheng, Adv. Mater. 25 (2013) 1296–1300.